Geophys. J. Int. (2003) **154,** 196–204

Origin of upper-mantle seismic scattering – evidence from Russian peaceful nuclear explosion data

Lars Nielsen,[1] Hans Thybo,[1] Alan Levander[2] and Leonid N. Solodilov[3]

[1] *Geological Institute, University of Copenhagen, Øster Voldgade* 10, DK-1350 *Copenhagen K, Denmark. E-mail: ln@seis.geol.ku.dk*
[2] *Department of Earth Science, Rice University,* 6100 *Main Street, Houston, TX* 77005-1892, *USA*
[3] *GEON Centre,* 4 *Chisty Lane, Moscow,* 119034 *Russia*

Accepted 2003 February 18. Received 2003 February 11; in original form 2001 July 18

SUMMARY

Detailed interpretation of upper-mantle scattered waves recorded in the 800–1400 km offset range of four reversed 'peaceful nuclear explosion' seismic sections along the 3500 km long profile Kraton in Russia has revealed an ∼85 km thick seismically inhomogeneous low-velocity zone below the 8° discontinuity at ∼100 km depth. The scattered waves make up a wave train of high amplitude that decreases in duration from ∼8 s at 800 km offset to ∼4 s at 1400 km offset. 2-D elastic finite-difference modelling of the seismic wavefield has previously shown that the inhomogeneous zone from ∼100 to ∼185 km depth may be described by continuous, random velocity fluctuations represented by an exponential medium with a horizontal correlation length of 5–10 km, a vertical correlation length of <5 km and a standard deviation of ∼2 per cent of the average background velocity value. Here, we demonstrate that other proposed velocity fluctuations in the lower crust and in the uppermost mantle from the Moho to ∼100 km depth cannot explain the observed scattered phases. Our study shows that upper-mantle velocity fluctuations below the 8° discontinuity at 100 km depth are needed in order to explain the observed seismic wavefield, and that they lead to scattering that is significantly different from the scattering caused by the fluctuations at shallower levels.

Key words: 8° discontinuity, scattering, seismic modelling, seismic waves, synthetic seismograms, upper mantle.

INTRODUCTION

Global seismic discontinuities that are identified in continental areas include the Mohorovičić discontinuity (Moho) between the crust and mantle, the 8° discontinuity at ∼100 km depth (Thybo & Perchuć 1997), the upper boundary of the transition zone at around 400 km depth (Jeffreys 1936) and the 660 km discontinuity (Niazi & Anderson 1965). Other discontinuities that are often interpreted in the upper mantle beneath continents are the Lehmann discontinuity at approximately 210 km depth (Lehmann 1964) and the 520 km discontinuity (Shearer 1993; Egorkin 1997).

Complicated wave patterns observed in high-resolution, controlled-source, wide-angle and deep normal-incidence seismic data sets are linked to small-scale inhomogeneities embedded in the crust and mantle between the major discontinuities. Levander & Holliger (1992) show that scattered seismic arrivals observed in southern Germany are in agreement with a model in which the lower crust contains small-scale velocity fluctuations, as observed in the Ivrea zone, where lower crustal rocks are exposed to the surface. According to Tittgemeyer *et al.* (1996) and Ryberg *et al.* (2000), the so-called teleseismic P_n phase observed to large offsets along 'peaceful nuclear explosion' (PNE) profile Quartz (Fig. 1) indicates that the uppermost mantle from Moho to approximately 100 km depth contains thin, horizontally elongated velocity anomalies. However, Morozov *et al.* (1998), Morozov & Smithson (2000) and Nielsen *et al.* (2003) suggest that these seismic arrivals should rather be understood as whispering-gallery phases that are influenced by crustal scattering. Based on a global investigation of several high-resolution long-range seismic sections, Thybo & Perchuć (1997) proposed an upper-mantle model for continental areas in which an approximately 100 km thick zone between the 8° discontinuity and the Lehmann discontinuity contains seismic scatterers. The average velocity of this zone is slightly reduced compared with the surrounding mantle, which is explained by this part of the upper mantle being partially molten. Nielsen *et al.* (2002) show that delayed and scattered upper-mantle *P* waves observed along the PNE profile Kraton (Fig. 1) may be explained by an inhomogeneous low-velocity zone situated at ∼100–185 km depth.

Based on 2-D visco-elastic finite-difference modelling, we calculate the seismic wavefield response of crustal and upper-mantle models, which contain stochastic velocity fluctuations. We show that velocity fluctuations between 100 and 185 km depth lead to scattered phases that are fundamentally different from those that result from other suggested velocity anomalies in the lower crust

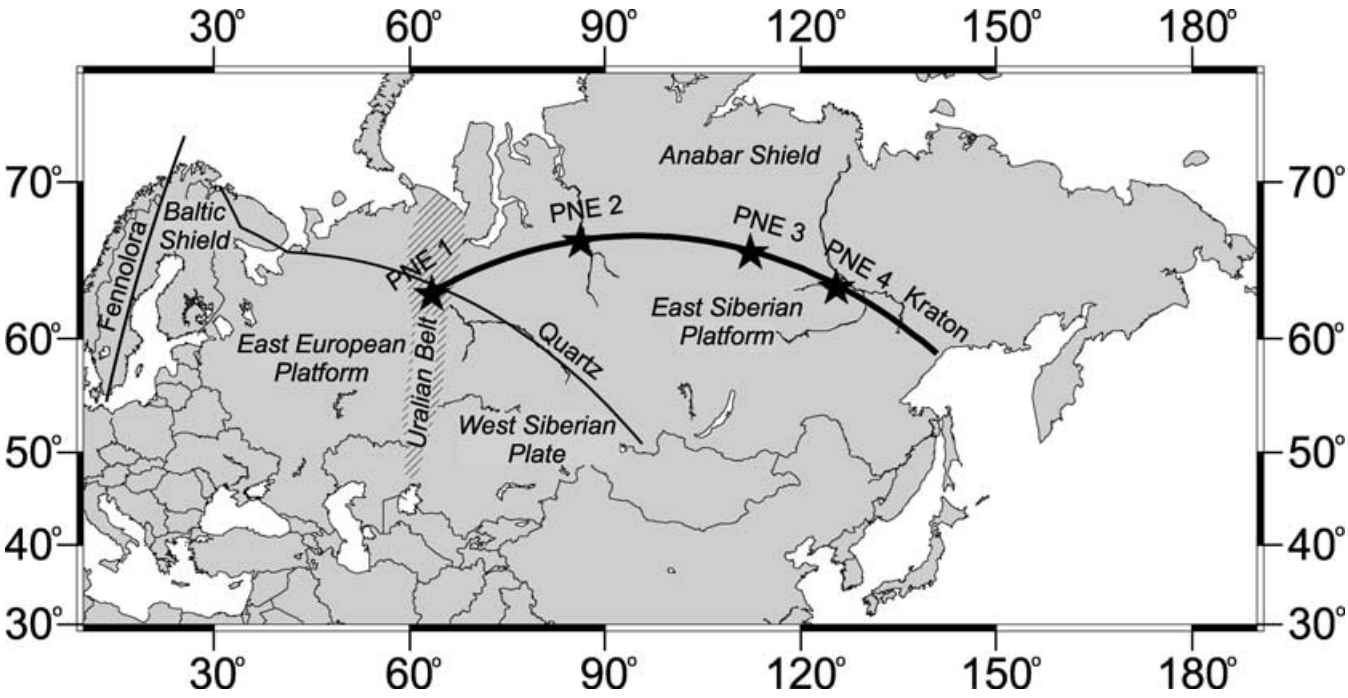

Figure 1. Location map of profile Kraton. The four stars show the locations of the PNE shot points. The scattered field is observed on all four shots. The locations of deep seismic profiles Fennolora and Quartz are shown by thin lines. The names of the main tectonic provinces are given in italic.

and uppermost mantle to ∼100 km depth. The studies are based on seismic data collected along the 3500 km long PNE profile Kraton, and we show that only the model with a heterogeneous low-velocity zone below the 8° discontinuity can explain the observed coda.

OBSERVED SCATTERED UPPER-MANTLE PHASES

Scattered mantle phases of high amplitude behind the first arrivals are mainly observed at offsets >800 km in the four PNE seismic sections along profile Kraton. The main frequency of these phases is ∼2 Hz for PNEs 1, 2 and 4 (Fig. 2) and ∼3 Hz for PNE 3 (*cf.* Nielsen *et al.* 2001). In combination with the average receiver spacing of ∼15 km, the 2 Hz seismic signals permit high-resolution investigation of upper-mantle structures. The important characteristics of the scattered arrivals are as follows.

(1) The scattered arrivals are mainly observed in the ∼800–1400 km offset range.

(2) The wave trains of high-amplitude scattered phases decrease in duration from approximately 8 s at ∼800 km offset to ∼4 s at ∼1400 km offset. The coda duration is ∼1.5 times the expected time interval between the reflections from 100 and 185 km depth.

(3) With recordings made at ∼15 km station spacing the scattered arrivals show little lateral correlation and individual phases cannot be confidently identified in the up to 8 s long time window in which the scattered waves appear.

These key observations are consistently made in all four Kraton record sections. Only weak scattering is observed directly behind the first arrivals at offsets <800 km, although a coda of up to 2–3 s duration is evident. Delays of up to ∼1–2 s are observed at 900–1000 km (∼8°) offset in all four sections recorded along profile Kraton (Fig. 2; Nielsen *et al.* 2001). These delays constrain an ∼85 km thick inhomogeneous low-velocity zone below the 8° discontinuity at ∼100 km depth (Nielsen *et al.* 1999). It is unlikely that delays caused by lateral variations in the velocity field always appear at 900–1000 km offset in the seismic sections along the line. Thus, the delays should be explained by the vertical mantle velocity structure.

Beyond ∼1800 km offset a weak, linear phase, the Lehmann refraction, from below the zone of scattering is observed. Strong reflections from approximately 350 km depth and the top of the transition zone (∼410 km) are observed at offsets larger than 1500 km (*cf.* Thybo *et al.* 1997).

FINITE-DIFFERENCE MODELLING OF SCATTERED PHASES

Based on the results of Nielsen *et al.* (1999), we subdivide the upper mantle down to the 400 km discontinuity into three principal layers: (1) from 35 to 100 km depth the velocity increases from 8.04 to 8.44 km s^{-1}; (2) from the 8° discontinuity at 100–185 km depth the vertical velocity gradient is almost zero and the background velocity is slightly reduced compared with the surrounding layers (Nielsen *et al.* 1999) (here we have chosen a constant velocity of 8.44 km s^{-1} for this interval); (3) below 185 km depth (the Lehmann discontinuity) the velocity gradient is positive from a velocity of 8.44 km s^{-1}. In order to investigate the origin of the observed scattering, we consider three different types of stochastic velocity models: (1) a model in which the lower crust contains velocity fluctuations as described by Holliger & Levander (1992) (Fig. 3a); (2) a model containing thin, horizontally elongated velocity anomalies in the uppermost mantle from 35 to 100 km depth as proposed by Ryberg *et al.* (2000) (Fig. 3b); (3) a model where the 100–185 km depth range contains random velocity fluctuations represented by a medium that follows a von Karman distribution function with a Hurst number of 0.3, a horizontal correlation length of 10 km, a vertical correlation length of 5 km and a standard deviation of 2 per cent of the average background velocity value (*cf.* Nielsen *et al.* 2002) (Fig. 3c); (4) a model

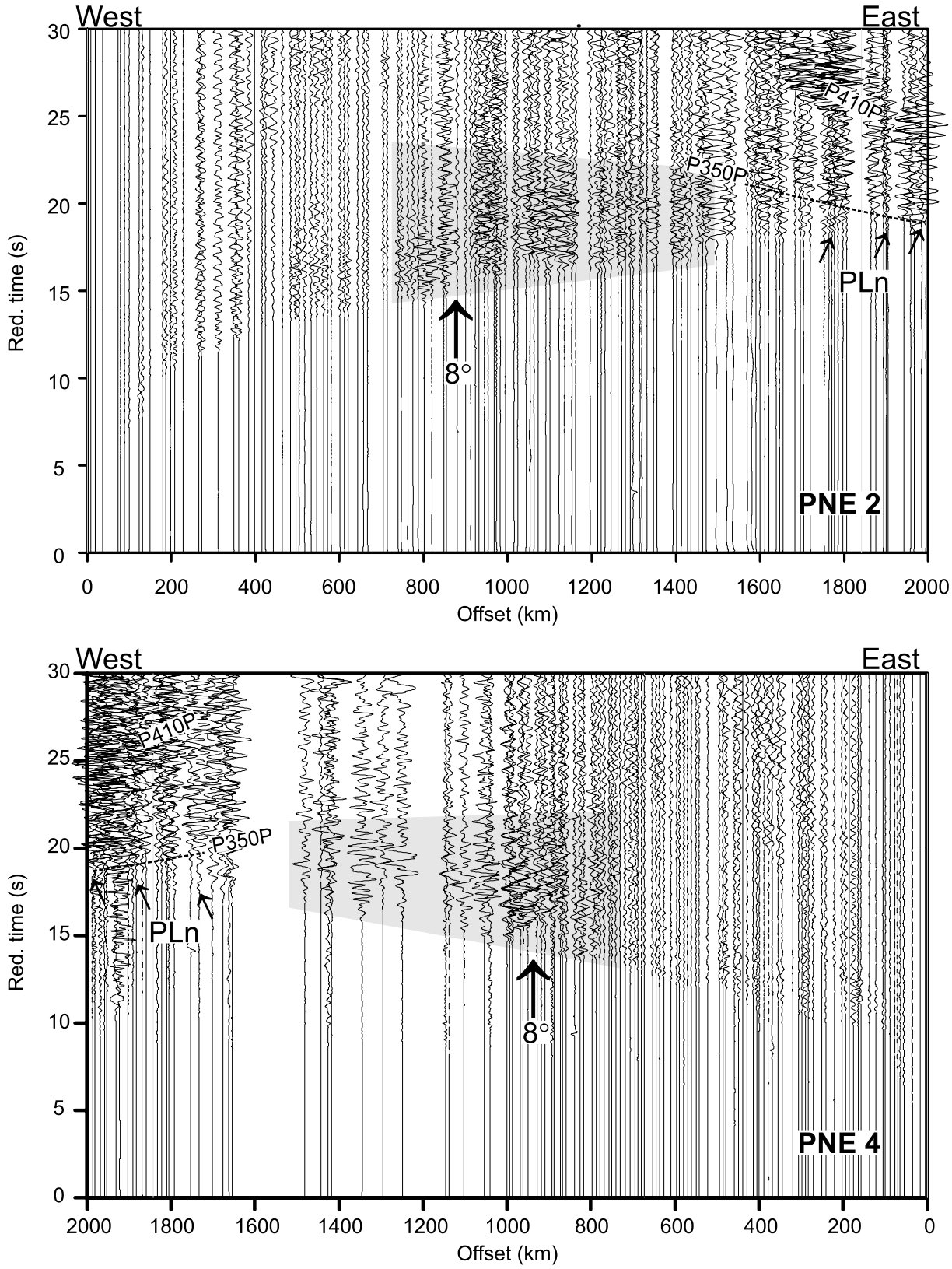

Figure 2. Data recorded along the Kraton profile from PNEs 2 and 4. The data sections are shown in reduced traveltime format (reduction velocity is 8.7 km s^{-1}). The scattered arrivals observed in the 800–1400 km offset range are indicated by grey rectangles. Amplitudes are scaled proportional to offset. The vertical arrows mark the traveltime delays associated with the 8° discontinuity. Tilted arrows identify the refraction from below the Lehmann discontinuity, *PLn*. Note that the observed scattered phases do not interfere with the reflected arrivals from the top of the transition zone (P410P). The dotted line indicates a reflection from approximately 350 km depth (*cf.* Thybo & Perchuć 1997).

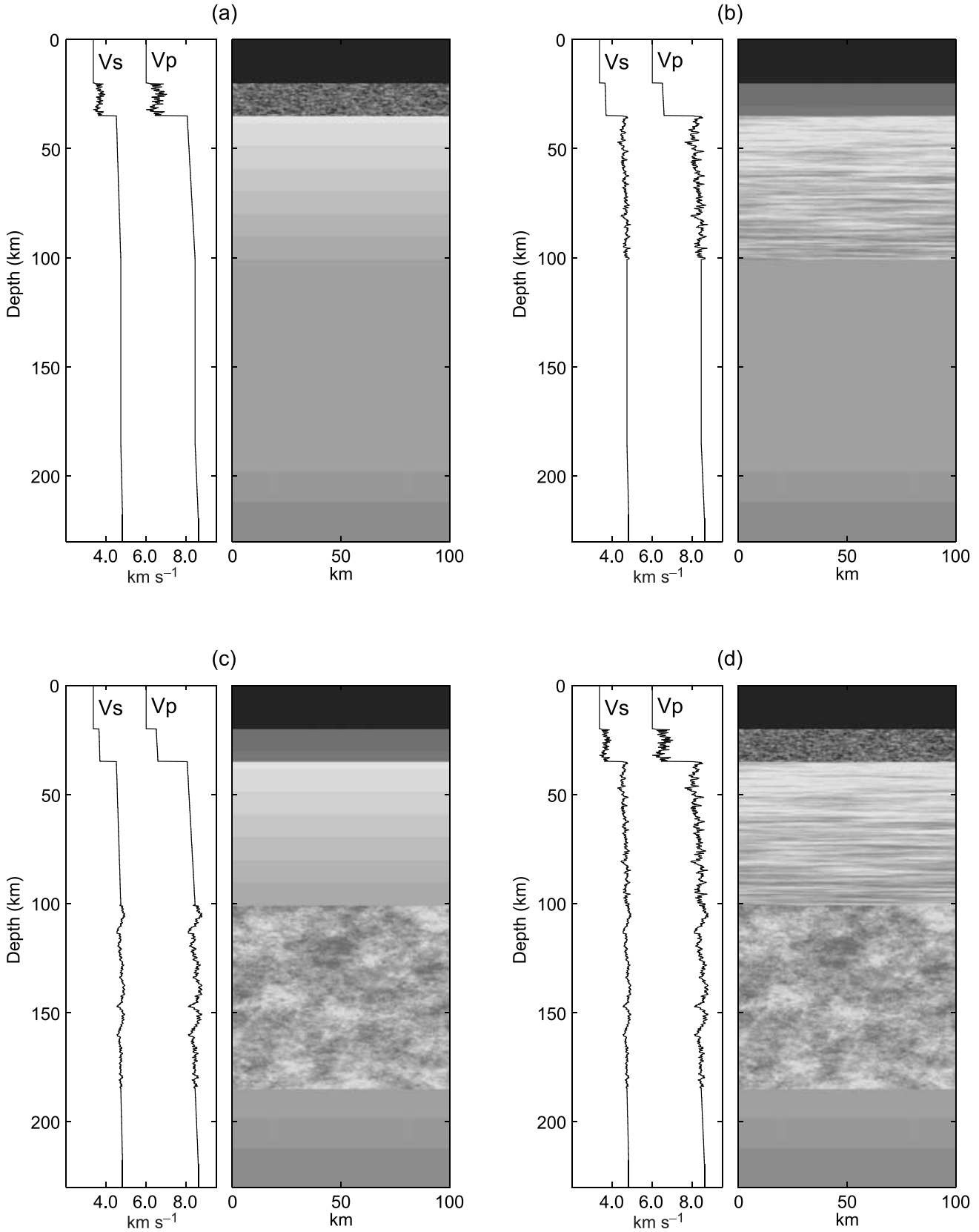

Figure 3. Images of the models investigated in this study. Only 100 km wide portions of the 2000 km wide models are shown. 1-D V_p- and V_s-profiles shown to the left of the model images are extracted from the 2-D models at a distance of 3.4 km. (a) Model containing lower crustal velocity fluctuations according to Holliger & Levander (1992). (b) Model containing thin, elongated velocity fluctuations from the Moho to 100 km depth according to Ryberg *et al.* (2000). (c) Model containing fluctuations in the 100–185 km depth interval according to Nielsen *et al.* (2002). (d) Model combining all types of fluctuations. In all four models, the background *P*-wave velocity structure is based on the tomographic image found by Nielsen *et al.* (1999).

which combines all the crustal and upper-mantle heterogeneities described above (Fig. 3d). We use the flat-Earth approximation in order to account for sphericity of the Earth (Aki & Richards 1980). The model values given above and shown in Fig. 3 have been transformed using this approximation, and, therefore, they are slightly larger than the actual spherical-Earth values.

We use the visco-elastic finite-difference algorithm described by Robertsson *et al.* (1994) for calculating the wavefield in the highly inhomogeneous models. The models have been sampled with a horizontal and vertical grid spacing of 170 m. In order to maintain accuracy of the finite-difference calculations we only propagate signals with frequencies up to 4 Hz (five gridpoints/minimum shear wavelength) on the grid. The synthetic seismograms are calculated in time steps of 7 ms. Hence, we need to calculate 47 150 time steps in order to obtain 330 s long seismic records. The size of the models is 11 765 × 1471 gridpoints (2000 × 250 km). Edge-effects, such as reflections from the sides of the model, are suppressed by a 30 gridpoint wide zone of high attenuation ($Q_p = Q_s = 2$), which surrounds the model grid. In all models, we relate *S*-wave velocity and density to *P*-wave velocity by assuming a Poisson ratio of 0.25 for the crust and 0.27 for the mantle. Density is linked to *P*-wave velocity using the linear relationship of Birch (1961). For the visco-elastic calculations, we have assigned *Q*-values to the crust and mantle. In the upper 5 km of the crust we have chosen low *Q*-values ($Q_p = 100$ and $Q_s = 60$) to account for the damping effects of sediments and faulted upper crystalline basement structures, and heuristically, the effects of scattering attenuation resulting from small topography. From 5 to 20 km depth, we select $Q_p = 200$ and $Q_s = 125$. In the remaining crustal column, $Q_p = 500$ and $Q_s = 300$. In the mantle layer from Moho to 100 km depth and in the layers below 185 km depth we select Q_p- and Q_s-values of 1000 and 600, respectively. The reduced background *Q*-values ($Q_p = 800$ and $Q_s = 450$) from 100 to 185 km are selected because this depth interval has been suggested to contain small amounts of molten material (Thybo & Perchuć 1997).

The calculated visco-elastic seismic wavefield response of the background model with lower crustal scatterers (Fig. 3a) is shown in Fig. 4(a). The seismic arrivals of this section include: the crustal refraction (*Pg*), the crust–mantle reflection (*PmP*), the upper-mantle refracted wave (*P*), the Lehmann refraction (*PLn*) and the whispering-gallery phase (WG) propagating as multiple refractions along the underside of Moho (*cf.* Morozov & Smithson 2000; Nielsen *et al.* 2003). The small-scale lower crustal fluctuations mainly result in scattered phases in front of the *PmP* reflection at short offsets. They also add a very weak coda of scattered phases to all mantle phases. These scattered arrivals do not match the three key observations because: (1) the coda to the 2 Hz mantle signals is very weak and cannot account for the up to ∼8 s long wave train of high amplitude beyond 800 km offset and (2) the coda already appears at short offsets (<200 km) and is not mainly restricted to the 800–1400 km offset range.

The seismic section of Fig. 4(b) is the wavefield response of the model, which includes scatterers from the Moho to 100 km depth (Fig. 3b). Clearly, the upper-mantle fluctuations from 35 to 100 km depth give rise to scattered arrivals of significant amplitude, which trail the first arriving mantle waves. However, these scattered phases do not fit the observed scattering because: (1) the coda duration increases with offset, opposite to the observations; (2) at around 800 km offset the scattered wave trains only constitute a coda of approximately 3 s length; and (3) the coda is not mainly observed in the 800–1400 km offset range. Thus, the model of Ryberg *et al.* (2000), which was proposed to explain the origin of the high-frequency (>5 Hz) coda of the teleseismic P_n phase, cannot account for the scattered 2 Hz signals observed in the 800–1400 km offset range.

The seismic section in Fig. 4(c), which is calculated for the model containing fluctuations in the 100–185 km depth range (Fig. 3c), provides a better fit to the observed key features of the scattering: (1) the length of the scattered wave trains decreases from approximately 8 s at 800 km offset to around 4 s at 1400 km offset and (2) the scattered arrivals show only limited correlation and they are evenly distributed over the 4–8 s long time window, which follows the first arrivals.

The seismic response of the model, which combines all types of heterogeneity that we are concerned with, is shown in Fig. 4(d). This combined model does not provide a satisfactory fit to observations, because scattering attenuation in the zone from the Moho to 100 km depth reduces the scattering that can be observed from below the 8° discontinuity. Therefore, our preferred model for the mantle below profile Kraton does not include the heterogeneous zone proposed by Ryberg *et al.* (2000). Ryberg *et al.* (2000) argue that the upper mantle must include a ∼100 km thick, strongly heterogeneous zone below Moho in order to explain the characteristics of the teleseismic P_n, which is observed to offsets of more than 3000 km on PNE profiles Quartz and Ruby. However, new visco-elastic waveform modelling results show that the teleseismic P_n may be explained simply by a combination of an inhomogeneous lower crust and an uppermost mantle with a positive vertical velocity gradient (Nielsen *et al.* 2003).

DISCUSSION

Seismic scattering and low velocities below ∼100 km depth are reported from investigations of other high-resolution seismic data sets in the Russian and adjacent areas. Wenzel *et al.* (1997) and Tittgemeyer (1999) interpreted irregular first arrivals observed at offsets >800 km of the PNE seismic sections of profiles Quartz and Ruby (Fig. 1) to be the result of seismic scattering below ∼100 km depth. Ryberg *et al.* (1996) observe first arrival traveltime delays of approximately 2.5 s at 800–900 km offset in the PNE recordings along profile Quartz, which they interpret as being caused by low-velocity zones in the depth intervals of ∼105–130 and ∼150–180 km along the northernmost and the southernmost halves of this profile, respectively. From traveltime inversion, Morozova *et al.* (1999) identify a low-velocity zone between ∼100 and ∼170 km depth in the central part of the mantle beneath profile Quartz. Reflectivity modelling of seismic arrivals detected along the ∼2100 km long Fennolora profile (Fig. 1) has revealed a strongly heterogeneous mantle layer from ∼100 to ∼150 km depth beneath the Baltic Shield (Perchuć & Thybo 1996). Tomographic inversion of first *P*- and *S*-wave arrivals observed along the Fennolora profile identifies a low-velocity layer with a high V_p/V_s and a low *Q*-value for *S*-wave propagation in the same depth range (Abramovitz *et al.* 2002). Thus, the modelling results reported here may apply to a large part of the mantle below Russia and the Baltic Shield.

The scattered wavefield observed from 800 to 1400 km offset in the Kraton records is seen on seismic sections from widely distributed shot points. Therefore, they cannot result from near-surface effects. We have demonstrated that neither lower crustal nor uppermost mantle heterogeneity from Moho to ∼100 km depth can account for the characteristics of the scattered wavefield. A heterogeneous, low-velocity zone between 100–185 km reproduces the characteristics of the wavefield. Based on stochastic modelling, Nielsen

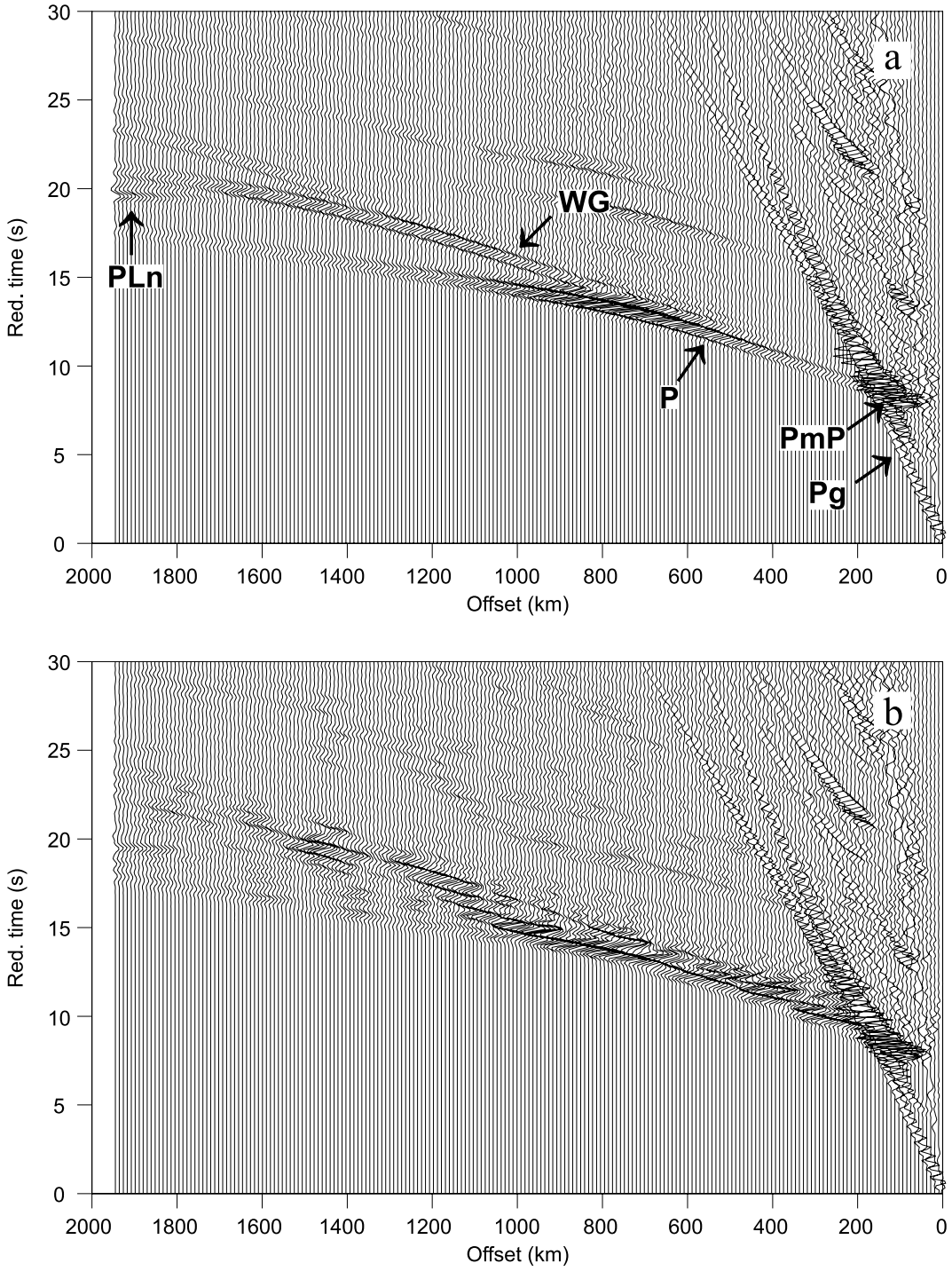

Figure 4. Calculated data sections shown in the same reduced traveltime format and with the same amplitude scaling as the observed data of Fig. 2. (a) Seismic response of the model containing velocity fluctuations in the lower crust (Fig. 3a). Annotated phases are: refraction from the crust (*Pg*); first arriving *P*-wave from the upper mantle (*P*); the whispering-gallery phase (WG); refraction from below the Lehmann discontinuity at 185 km depth (*PLn*). (b) Seismic response of the model containing velocity fluctuations from the Moho to 100 km depth (Fig. 3b). (c) Seismic response of model containing velocity fluctuations below the 8° discontinuity (Fig. 3c). (d) Seismic response of the model which includes heterogeneity in the lower crust, in the uppermost mantle from the Moho to 100 km depth and from 100 to 185 km depth (Fig. 3d).

et al. (2002) investigate how the choice of the spatial correlation parameters influence the characteristics of the modelled scattering from the 100–185 km depth interval. For continuous, exponentially correlated velocity fluctuations with a standard deviation of 2 per cent of the average background velocity, they find that the best fit to the observed scattered arrivals is obtained when the horizontal correlation is 5–10 km and the vertical correlation length is <5 km. For the studied mantle phases with a centre frequency of $\sim$2 Hz, the Fresnel radius at 150 km depth is of the order of 50 km. Thus, the actual geological structures that give rise to the scattering are below the resolution limit of the seismic data, and the observed scattered phases are caused by interference between the response of many

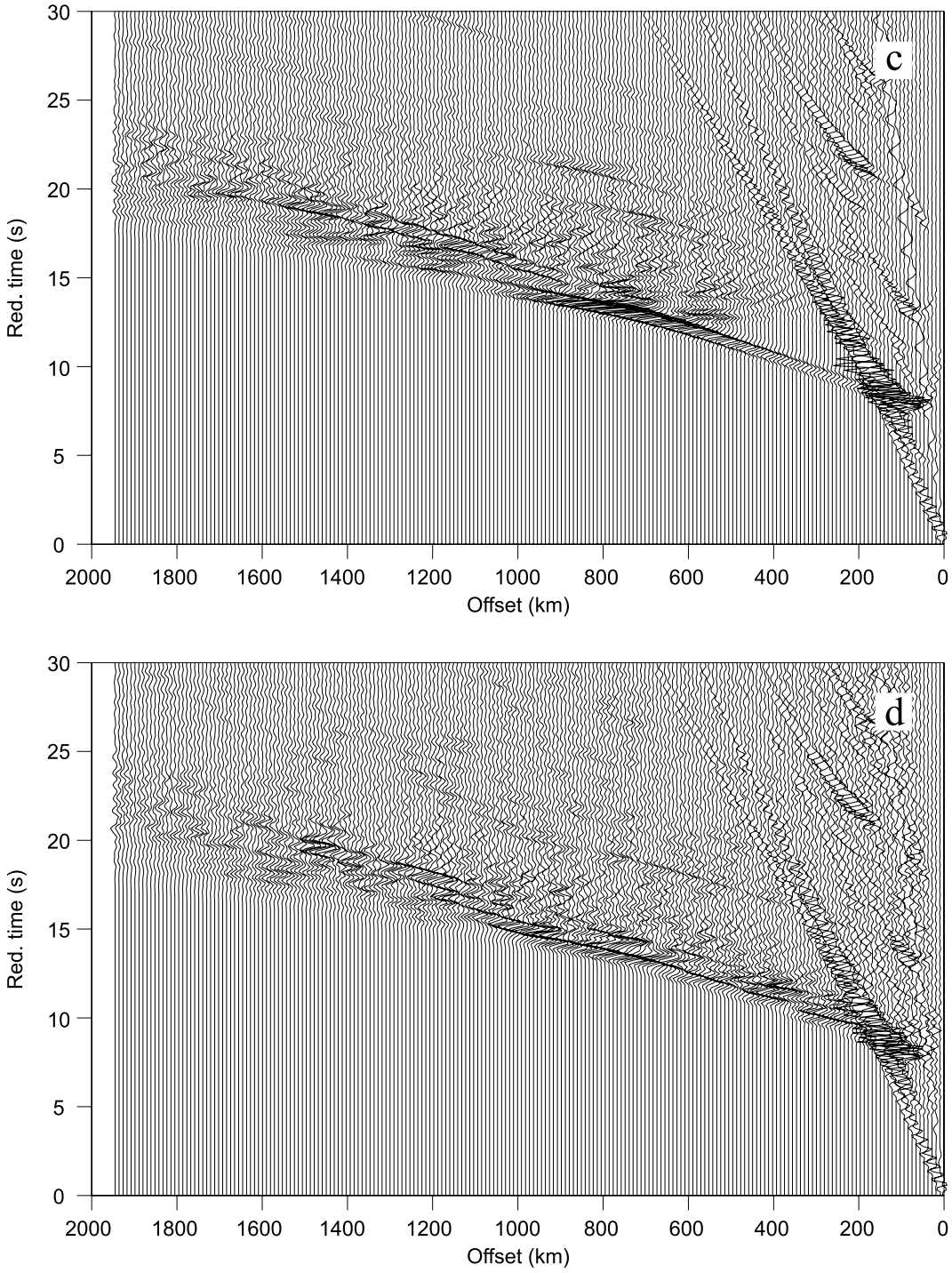

Figure 4. (*Continued*.)

scatterers. The scatterers are comparable to the wavelength of the input signal, as 2 Hz waves have a wavelength of approximately 4.25 km in this region. In Fig. 5, snapshots of the seismic wavefield propagating through a model, which contains scatterers in the 100–185 km depth range, are shown. At early times ($t = 21.775$ s), the wavefield has only propagated through a small part of the scattering zone. The scattered phases are of relatively small amplitude, and the wave front is only slightly undulating. The wavefield gradually becomes more scattered as it propagates further through the model. At $t = 91.455$ s, when the wave front has propagated to almost 800 km offset, the secondary arrivals have higher amplitude than the first arrivals and the wave front has become very irregular.

The observed scattering and the low average velocities in the 100–185 km depth interval may be explained by the existence of small amounts of partially molten material in this zone (Thybo & Perchuć 1997). According to Sato *et al.* (1989), up to 6 per cent reduction in the velocity of the upper-mantle rock should be expected at the solidus temperature, a reduction that gradually increases from ∼85 per cent of the solidus temperature. Thus, small partially molten bodies embedded in solid-state rocks of higher

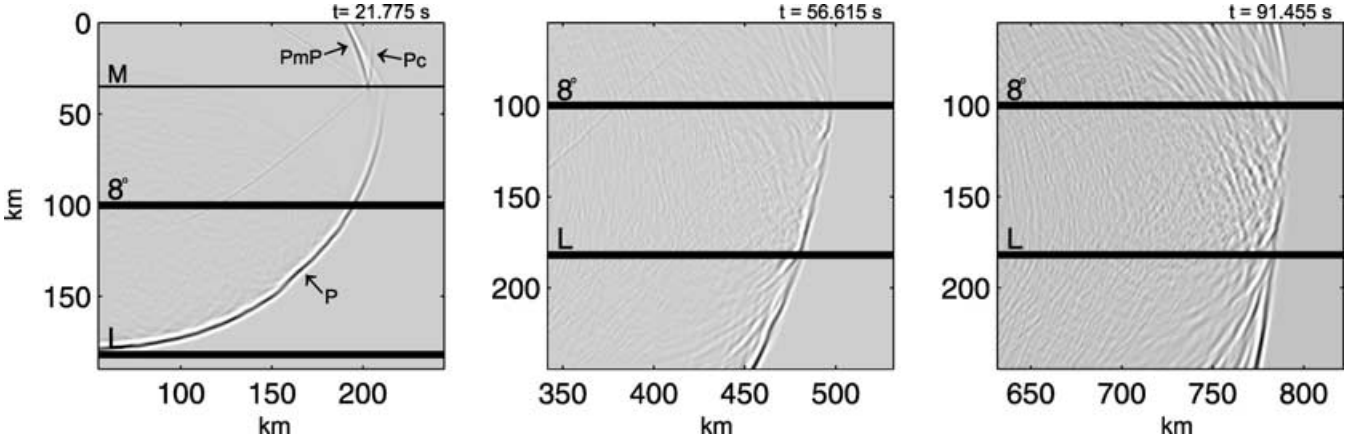

Figure 5. Snapshots taken at three different times, *t*, after shot. The seismic wavefield propagates through the model which incorporates heterogeneity from 100 to 185 km depth (Fig. 3c). The source is located at 56.28 km model distance. The thin black line shows the position of the Moho. Thick black lines indicate the 8° discontinuity and the Lehmann discontinuity. *P*, *P*-wave front; P_c, crustal refraction; *PmP*, Reflection from the crust–mantle boundary (modified after Nielsen *et al.* 2002).

velocity could lead to significant scattering of the seismic wavefield. As discussed by Nielsen *et al.* (2002), rheological weakening and low average velocities caused by high subsolidus temperatures combined with randomly distributed small-scale anisotropic bodies each having different velocities in the direction of wave propagation may also explain the existence of the low-velocity scattering zone, without melts being present. However, we see no viable explanation as to why such phenomena should always occur from ∼100 km depth. Possible mineralogical changes in the upper mantle may also lead to scattering. From geochemical studies, Griffin *et al.* (1996) propose that the mantle lithosphere in the central part of the Siberian kimberlite province is strongly layered. They suggest that depleted lherzolites predominate to a depth of approximately 150 km, while harzburgites comprise up to 60 per cent of the rock volume in the 150–180 km depth range.

Subhorizontal reflections have been detected at ∼25 and ∼35–44 s traveltime in the deep normal-incidence URSEIS data section collected across the southern Urals (Steer *et al.* 1998) and at ∼22–25 s traveltime on crossing marine seismic reflection profiles from the southeastern North Sea (MONA LISA Working Group 1997). If the heterogeneous low-velocity zone below ∼100 km depth is actually partially molten then the reflectivity at ∼22–25 s traveltime (∼80–90 km depth) might represent material that has solidified above this zone. The normal-incidence reflectivity detected at ∼35–44 s (>150 km depth) may represent reflectors inside the ∼85 km thick heterogeneous zone below the 8° discontinuity or at its base.

Our preferred model (Fig. 3c) incorporates a heterogeneous medium from 100 to 185 km depth, which is described by a von Karman distribution function with a Hurst number of 0.3. It has been noted that von Karman distribution functions exhibit self-affine characteristics above their corner wavenumber (e.g. Holliger & Levander, 1992).

CONCLUSIONS

Based on scattered arrivals observed in the PNE data of profile Kraton and visco-elastic finite-difference calculations of the seismic wavefield we draw the following conclusions.

(1) In order to fit scattered arrivals consistently observed in the 800–1400 km offset range of the PNE seismic sections along profile Kraton, we must incorporate an ∼85 km thick scattering layer below the 8° discontinuity at ∼100 km depth.

(2) Models containing continuous stochastic velocity fluctuations in the 100–185 km depth range lead to scattered phases that are significantly different from the scattered arrivals caused by inhomogeneities in the crust and uppermost mantle above ∼100 km depth. In particular, they approximately follow the kinematics of waves reflecting from the top and bottom of the zone across the offset range, but appear in a window approximately 1.5 times as long. Waves scattered in the uppermost mantle appear with different kinematics from the observed scattered field.

(3) Crustal effects cannot explain the observed scattered waves that we are concerned with in this study.

(4) The previously suggested mantle heterogeneity from the Moho to ∼100 km depth does not fit the key characteristics of the observed scattering. The fit to observations deteriorates if this zone is included on top of the heterogeneous layer from 100 to 185 km depth because the wavefield is attenuated in the scattering zone from the Moho to 100 km depth. Hence, our preferred model for the mantle below profile Kraton does not include heterogeneity from the Moho to 100 km depth.

ACKNOWLEDGMENTS

This research was carried out as part of the project Seismic-Tectonophysical Studies of the Tectosphere, which is funded by the Carlsberg Foundation and the Danish Natural Science Research Council. The visco-elastic waveform calculations were performed on the SGI Origin 2000/64 parallel computer of DCSC, Denmark, and the 20-processor SUN ES6500 of the Center for Computational Geophysics, Department of Earth Science, Rice University, Houston, Texas, USA. The digital data for PNE profile Kraton were kindly made available by the GEON, Moscow. We are grateful to Johan Robertsson for providing the visco-elastic code. Two anonymous referees provided valuable comments to an earlier version of this paper.

REFERENCES

Abramovitz, T., Thybo, H. & Perchuć, E., 2002. The 8° discontinuity in the upper mantle beneath the Baltic shield interpreted from Fennolora *P*- and *S*-wave seismic data, *Tectonophysics,* **358,** 151–174.

Aki, K. & Richards, P.G., 1980. *Quantitative Seismology: Theory and Methods,* vols I, II, Freeman, San Francisco.

Birch, F., 1961. The velocity of compressional waves in rocks to 10 kilobars, Part 2, *J. geophys. Res.,* **66,** 2199–2224.

Egorkin, A.V., 1997. Evidence for 520-km discontinuity, in *Upper Mantle Heterogeneities from Active and Passive Seismology,* pp. 51–62, ed. Fuchs, K., NATO ASI Series, Kluwer, Dordrecht.

Frankel, A., 1989. Review of numerical experiments on seismic scattering, *Pure appl. Geophys.,* **131,** 639–683.

Fuchs, K., 1983. Recently formed elastic anisotropy and petrological models for the subcrustal lithosphere in southern Germany, *Phys. Earth planet. Inter.,* **31,** 93–118.

Griffin, W.L., Kaminsky, F.V., Ryan, C.G., O'Reilly, S.Y., Win, T.T. & Ilupin, I.P., 1996. Thermal state and composition of the lithospheric mantle beneath the Daldyn kimberlite field, Yakutia, *Tectonophysics,* **262,** 19–33.

Holliger, K. & Levander, A.R., 1992. A stochastic view of lower crustal fabric based on evidence from the Ivrea zone, *Geophys. Res. Lett.,* **19,** 1153–1156.

Jeffreys, H., 1936. The structure of the earth down to the 20° discontinuity, *Mon. Not. R. Astron. Soc. Geophys. Suppl.,* **3,** 401–422.

Lehmann, I., 1964. On the travel times of *P* as determined from nuclear explosions, *Bull. seism. Soc. Am.,* **54,** 123–139.

Levander, A.R. & Holliger, K., 1992. Small-scale heterogeneity and large-scale velocity structure of the continental crust, *J. geophys. Res.,* **97,** 8797–8804.

MONA LISA Working Group, 1997. MONA LISA—deep seismic investigations of the lithosphere in the south-eastern North Sea, *Tectonophysics,* **169,** 1–19.

Morozov, I.B. & Smithson, S., 2000. Coda of long-range arrivals from nuclear explosions, *Bull. seism. Soc. Am.,* **90,** 929–939.

Morozov, I.B., Morozova, E.A., Smithson, S. & Solodilov, L., 1998. On the nature of the teleseismic P_n phase observed on the ultralong-range profile QUARTZ, Russia, *Bull. seism. Soc. Am.,* **88,** 62–73.

Morozova, E.A., Morozov, I.B., Smithson, S. & Solodilov, L., 1999. Heterogeneity of the uppermost mantle beneath Russian Eurasia from the ultra-long-range profile Quartz, *J. geophys. Res.,* **104,** 20 329–20 348.

Niazi, M. & Anderson, D.L., 1965. Upper mantle structure of western North America from apparent velocities of *P* waves, *J. geophys. Res.,* **70,** 4633.

Nielsen, L., Thybo, H. & Solodilov, L., 1999. Seismic tomographic inversion of Russian PNE data along profile Kraton, *Geoph. Res. Lett.,* **26,** 3413–3416.

Nielsen, L., Thybo, H. & Egorkin, A.V., 2001. Constraints on reflective bodies below the 8° discontinuity from reflectivity modelling, *Geophys. J. Int.,* **145,** 759–770.

Nielsen, L., Thybo, H. & Egorkin, A.V., 2002. Implications of seismic scattering below the 8° discontinuity along PNE profile Kraton, *Tectonophysics,* **358,** 135–150.

Nielsen, L., Thybo, H., Morozov, I.B., Smithson, S.B. & Solodilov, L., 2003. Teleseismic P_n arrivals: influence of upper mantle velocity gradient and crustal scattering, *Geophys. J. Int.,* **153,** F1–F7.

Perchuć, E. & Thybo, H., 1996. Upper mantle *P*-wave velocity model for the Baltic Shield, *Tectonophysics,* **253,** 227–245.

Robertsson, J.O.A., Blanch, J.O. & Symes, W.W., 1994. Viscoelastic finite-difference modeling, *Geophysics,* **59,** 1444–1456.

Ryberg, T., Wenzel, F., Mechie, J., Egorkin, A.V., Fuchs, K. & Solodilov, L., 1996. Two-dimensional velocity structure beneath northern Eurasia derived from the super long-range seismic profile quartz, *Bull. seism. Soc. Am.,* **86,** 857–867.

Ryberg, T., Tittgemeyer, M. & Wenzel, F., 2000. Finite difference modelling of *P*-wave scattering in the upper mantle, *Geophys. J. Int.,* **141,** 787–800.

Sato, H., Sacks, I.S. & Murase, T., 1989. The use of laboratory velocity data for estimating temperature and partial melt fraction in the low-velocity zone: comparison with heat flow and electrical conductivity studies, *J. geophys. Res.,* **94,** 5689–5704.

Shearer, P.M., 1993. Global mapping of upper mantle reflectors from long-period *SS* precursor, *Geophys. J. Int.,* **115,** 878–904.

Steer, D.N., Knapp, J.H., Brown, L.D., Echtler, H.P., Péréz-Estaun, A. & Berzin, R., 1998. Deep structure of the continental lithosphere in an unextended orogen: an explosive source seismic reflection profile in the Urals (Urals Seismic Experiment and Integrated Studies (URSEIS 1995)), *Tectonics,* **17,** 143–157.

Thybo, H. & Perchuć, E., 1997. The seismic 8° discontinuity and partial melting in continental mantle, *Science,* **275,** 1626–1629.

Thybo, H., Perchuć, E. & Pavlenkova, N., 1997. Two reflectors in the 400 km depth range revealed from peaceful nuclear explosion seismic sections, in *Upper-Mantle Heterogeneities from Active and Passive Seismology,* pp. 97–104, ed. Fuchs, K., NATO ASI Series, Kluwer, Dordrecht.

Tittgemeyer, M., 1999. Streuung elastischer Wellen im oberen Erdmantel, *PhD thesis,* University of Karlsruhe, p. 131.

Tittgemeyer, M., Wenzel, F., Fuchs, K. & Ryberg, T., 1996. Wave propagation in a multiple-scattering upper-mantle—observations and modelling, *Geophys. J. Int.,* **127,** 492–502.

Wenzel, F., Fuchs, K., Tittgemeyer, M. & Ryberg, T., 1997. Small-scale heterogeneities of the upper-mantle, in *Upper Mantle Heterogeneities from Active and Passive Seismology,* pp. 215–224, ed. Fuchs, K., NATO ASI Series, Kluwer, Dordrecht.